Astron. Astrophys. 352, 167–176 (1999)

ASTRONOMY AND ASTROPHYSICS

Locating the emission line regions in polars

II. Doppler imaging of BL Hydri

R.E. Mennickent[1,⋆], **M.P. Diaz**[2], **and J. Arenas**[3]

[1] Dpto. de Física, Facultad de Ciencias Físicas y Matemáticas, Universidad de Concepción, Casilla 4009, Concepción, Chile (rmennick@stars.cfm.udec.cl)
[2] Instituto Astronômico e Geofísico, Universidade de São Paulo, CP9638, 010065-970, São Paulo, Brazil (marcos@binary.iagusp.usp.br)
[3] Department of Physics, Keele University, Keele, Staffordshire ST5 5BG, UK (jla@astro.keele.ac.uk)

Received 29 March 1999 / Accepted 4 October 1999

Abstract. Phase-resolved spectroscopic observations of BL Hyi obtained during the high mass transfer state are presented. The Hα, He I 5875 and He I 6678 emission line profiles are analyzed with the Doppler tomography technique. It is shown that these emissions arise from a single region in the accretion stream. No emission from the secondary star, either in the Hα or in the He I line, could be identified. The accretion column could not be detected on the tomographic reconstructions of the system. An orbital ephemeris based on the radial velocities of the Na I D emission line is derived, assuming a chromospheric origin in the secondary star. The spectroscopic observations provide a consistent picture of the accretion geometry in the system. Most of the optical emission line flux was found to be formed in a reservoir of low angular momentum gas filling a substantial fraction of the Roche lobe. Combining our results with literature data it was possible to constrain the absolute longitude of the magnetic axis in this classical polar.

Key words: stars: individual: BL Hyi – stars: novae, cataclysmic variables – stars: fundamental parameters – stars: evolution – stars: binaries: general

1. Introduction

1.1. About polars

Polars or AM Her stars are a subclass of magnetic cataclysmic variables with white dwarf surface magnetic field strength of the order of 10^8 Gauss. This strong field prevents the formation of an accretion disk around the white dwarf. Instead, the gas follows the field lines for distances shorter than the Alfven radius, being accreted at one (or both) magnetic poles of the white dwarf. In classical polars, the white dwarf rotation is synchronized with the orbital motion by the primary's magnetic field (see Warner 1995 and references therein for a review of AM Her stars). The most important lines seen in the optical spectrum of polars are the Balmer, He I, He II 4686 lines and the C III/N III blend. Typically the strengths of He II 4686 and Hβ are comparable and the spectra show flat Balmer decrements. The line profiles are strongly modulated with the binary period showing a generally complex shape, indicating the presence of many components, each with its own velocity amplitude. The presence of highly structured lines in polars are known since the early medium resolution spectroscopic studies of AM Her (Young & Schneider 1979) and EF Eri (Hutchings et al. 1982). However the large amount of information contained in the line profile modulations was not globally exploited until tomographic reconstructions were performed.

1.2. Previous Doppler tomograms of polars

Doppler tomography is just starting to be used as a diagnostic tool in the study of polars. It may be used as an additional resource in the discrimination between systems with and without discs in cases where only the emission from the ballistic stream is detected. In the particular case of polars, the comparative study of various emission line profiles is possibly the best method for probing the dynamics and physical properties of the stream, magnetic coupling region and the upper parts of the accretion column itself. Doppler tomography has also been proposed as a new tool for the mass determination of accreting binaries provided that an independent mass estimator can be used as a calibrator (Schwope et al. 1997).

Doppler tomograms of VV Pup (Diaz & Steiner 1994, paper I) showed that the line components map to well defined locations in the binary like the stream and the surface of the red dwarf. The emissivity of these line emission regions was quantified showing that the stream contributes to about 40% of the Hα flux while the illuminated secondary emission amount to 30% of the line. The remaining is possibly formed in the coupling region and the accretion column itself which on its turn contributes with a small amount (if any) of the observed line flux. Another well studied polar is HU Aqr, where three spectral components are clearly visible by mean of Doppler tomography (Schwope et al. 1997). The origin of at least two components could be located

Send offprint requests to: R.E. Mennickent

⋆ On leave in Harvard-Smithsonian Center for Astrophysics, 60 Garden St, MA 02138, Cambridge, USA

unequivocally (a) on the secondary star and (b) the ballistic part of the accretion. In addition, there is some marginal indication of emission produced in the magnetically funneled part of the gas flow. On the other hand, the eclipsing binary V 1309 Ori (RX J0515.6+0105) shows Doppler maps consistent with emission arising from the accretion stream and from the vicinity of the secondary star (Shafter et al. 1995). Finally, Tovmassian et al. (1999) claim the detection of all these three emission regions in the Doppler reconstructions of the polar RXJ0719.2+6557. The aforementioned cases contrast in many ways with the observations presented in this work.

1.3. About BL Hyi

This paper is aimed to investigate the line emission regions in the AM Her system BL Hyi. This object was discovered and identified by Agrawal et al. (1983). X-Ray observations reveal low and high states associated to changes in average visual magnitude switching between roughly $V = 15.3$ and 17.1 and characterized by both single-pole and two-pole accretion (Agrawal et al. 1983, Beuermann & Schwope 1989, Schwope et al. 1995, Ramsay et al. 1996). The system parameters and the moderate magnetic field strength (around 23 or 30 MG for the mean photospheric field, e.g. Wickramasinghe et al. 1984, Ferrario et al. 1996) are comparable with that of VV Pup, but BL Hyi has a cooler accretion area (e.g. Szkody et al. 1997). Although the accretion column and its cyclotron emission has been intensively studied using X-ray/UV data (Matt et al. 1998) and optical/IR polarimetry (Ferrario et al. 1996), there is no recent spectroscopic study of the system. In fact, the early phase-resolved spectroscopic observations that detected the structured and complex profile modulation in BL Hyi (Hutchings et al. 1985, Thorstensen et al. 1983, hereafter H85 and T83 respectively) were not followed by more detailed studies that could bring an interpretation of these profiles in terms of the kinematics of the gas located far away from the accretion shock.

BL Hyi does not present eclipses of the primary star nor independent detection of the red dwarf radial velocity. Therefore, a substantial uncertainty in the dipole position relative to the red dwarf is inevitable. However, the phase of minimum column angle with respect to the line of sight and the phase when the column direction is perpendicular to the line of sight were derived from polarimetric observations. The published phase scale is not absolute but depends on the photometric fiducial point (Schwope & Beuermann 1989 and Piirola et al. 1987).

In the next section we describe the observational techniques used to obtain and reduce our spectroscopic and photometric observations. In Sect. 3 we describe our results and discuss a consistent scenario for the system geometry. Finally we draw our conclusions in Sect. 4.

2. Observations and data reduction

2.1. Time resolved spectroscopy

Spectroscopic observations were conducted in the 1.5 m Ritchey-Chretien telescope of CTIO on October 1996 with the R-C spectrograph. The Loral CCD and grating # 35 tilted by an angle of 18.68 degree, combined with a slit width of one arc-second yielded a spectral resolution of 3.6 Å (164 km s^{-1} at Hα) and a spectral range of $\lambda\lambda$ 5205–7010 Å. He-Ar comparison images were taken typically in intervals of 30 minutes between several 5 min. science exposures. Additional calibrations like Flat Fields and Biases were taken during day time. The observations are summarized in Table 1.

Table 1. Log of spectroscopic observations. N is the number of spectra. HJD (-2450 300) at the start and the end of the night are given. Each spectrum has 300 s of exposure time.

Date(UT)	N	HJD_{start}	HJD_{end}
23/10/96	36	79.5118	79.6582
24/10/96	46	80.5112	80.7109
25/10/96	48	81.4958	81.6857
26/10/96	48	82.4909	82.6818

Image reductions were realized in the usual manner. First, the two dimensional frames were divided by the normalized Flat Field subtracting also the Bias using the IRAF[1] *ccdproc* routine. Afterwards, one dimensional spectra were extracted (subtracting the sky) and wavelength calibrated using the IRAF *doslit* package. About 14 He-Ar emission lines provided spectral calibration functions with typical rms of 0.04 Å (2 km s^{-1} at Hα).

Radial velocities (RVs) of the emission lines, referred to the Local Standard of Rest (V_{sun} = 20 km s^{-1}, $\alpha_{sun} = 18^h$ and $\delta_{sun} = +30^o$), were measured using the algorithm originally developed by Schneider & Young (1980), adopted by Shafter (1983) and refined by Horne et al. (1986). This method provides a robust diagnostic test for investigating the behavior of different profile sections during the orbital cycle. The method consists in to simultaneously shift two Gaussians of standard deviation σ_g (or alternatively full width at half maximum $FWHM_g$) and separation Δ along the emission profile until a velocity is found for which the convolved flux in both sides is the same. Changing Δ and $FWHM_g$ we can probe different velocity sections of every profile.

2.2. Differential photometry

Simultaneous, time-resolved photometric observations were obtained at the 0.6m Boller&Chivens telescope of LNA at Brasopolis, Brazil in October 25, 1996. These observations were taken using a liquid nitrogen cooled GEC CCD (770×1152) through a standard (Kron-Cousins) R filter. Differential photometry was performed using 4 field stars by a non-interactive IRAF script (LCURVE). Internal photometric uncertainties were smaller than 0.01 mag. The time resolution of 1 minute allowed the timing of the light curve raise to the bright phase,

[1] IRAF is distributed by the National Optical Astronomy Observatories, which are operated by the Association of Universities for Research in Astronomy, Inc., under cooperative agreement with the National Science Foundation

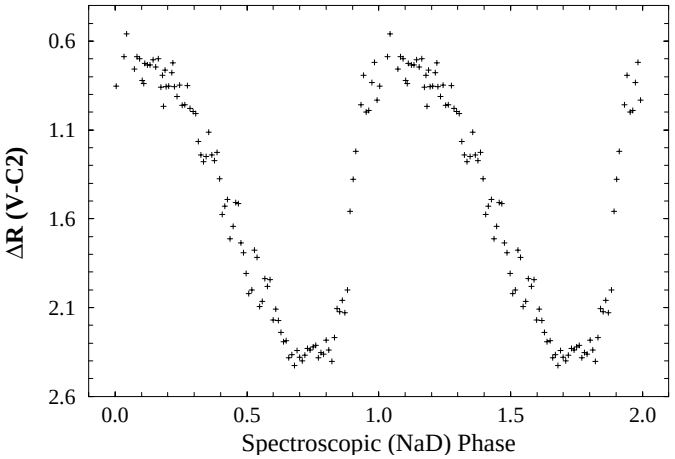

Fig. 1. Broad band (R_{KC}) simultaneous light curve folded using the ephemeris given by Eq. 2.

which is the fiducial photometric feature used in recently published ephemeris (see discussion in Szkody et al. 1997).

3. Results

3.1. The R light curve

We folded our differential magnitudes with the spectroscopic ephemeris derived in the next section. The light curve shows a strong $1\overset{\mathrm{m}}{.}7$ amplitude hump characterized by a steep rise from the faint phase and a slower decline (Fig. 1). The hump lasts by about 0.8 cycles (so called the bright phase hereafter). This is in close agreement with the figure of Pickles & Visvanathan (1983). The longer baseline of these authors (about 1 year) permitted to establish that the light curve does not repeat exactly, either in magnitude, shape or duration of maximum. However, they found that the deep minimum and the strikingly steep rise from minimum light accurately repeated cycle to cycle. The light curve can be interpreted in terms of the synchronous rotator model for the white dwarf. The steep rise marks the appearance of the column base and the bright spot in the white dwarf surface as they cross the primary's limb (Pickles & Visvanathan 1983).

For our data, the time of rise was found by fitting a low order polynomial curve to the steep slope in the light curve. The time of light curve crossing the level given by $[m_{faint} + m_{bright}]/2$ is:

$$T(rise) = HJD\ 2450381.5948(4) \quad (1)$$

This ephemeris can be used in a future long-term analysis aimed to improve the orbital period. Moreover, it will allow the phase comparison of our measurements with previous works that included simultaneous photometric observations.

3.2. Spectra and radial velocities

Trailed spectra of the main emission lines were constructed after binning the observations with the orbital period (Figs. 2a–c). They basically show a broad emission component and no signs of the narrow emission peak suggested in previous studies (T83 and H85). What is striking in our spectra is the presence of a weak line near He 5875 (Fig. 2d). The observed wavelength of this feature averages around 5893 Å. The behavior of this line contrasts with that observed in the Hydrogen and Helium lines. For instance, the phasing is different. Its flux is only 1% of Hα. During the orbital phases where the profile is not severely blended with He I an unresolved doublet or a double-peaked line can be observed (Fig. 3). When a double Gaussian deblending is applied to these phase averaged profiles we obtain an average separation between the components of 5.5(1.3) Å. These findings may suggest that the feature is Na I D (usually seen in absorption in normal low-mass main-sequence stars). The presence of a detectable Na I emission, however, may suggest that the secondary star in BL Hyi is chromospherically active. The absorption profile may be shallow relatively to the core reversal in high pressure chromospheres with intense activity (Short & Doyle 1998). The hypothesis of a highly active secondaries in short period cataclysmic variables is supported by the relatively high space densities found for X-ray bright, late M dwarfs among field stars (Fleming et al. 1995). The proposed D1+D2 lines are blended in our data and also immersed in the He I profile during a significant fraction of the orbital cycle. If the binned spectra shown in Fig. 3 are shifted by the observed Na I D radial velocities we obtain a reasonably well defined doublet profile (Fig. 4). An origin in the low temperature region of the stream is unlikely due to the large phase shift with respect to the other stream emission lines. In contrast, the low excitation line Ca II K have been observed (H85) with a phase shift of less than 0.1 cycles with respect to the Hydrogen and Helium lines. This may eventually indicate an origin of part of the Ca II K emission in the stream. However, a detailed study of the Ca II K radial velocity curve is needed to better clarify this point.

Other tentative identifications of this line are C II 5891 (although slightly displaced in wavelength) and C III 5894 (multiplet 20). These possibilities could not be confirmed with the data at hand. However, the C II 4267 line which is the strongest C II line seen in the optical spectra of cataclysmic variables is only marginally detectable in the spectrum of BL Hyi (Thorstensen et al. 1983). Other C II lines, namely C II 6780/83 and C II 5663, show flux upper limits that seem inconsistently low if the feature in 5893 Å is assumed to be C II 5891. These arguments suggest that the identification of the feature at 5893 Å as C II 5891 is unlikely. No C III lines could be identified in the spectrum except for the N III+C III complex at 4640–50 Å. The candidate line (C III 5894) is sometimes observed as a weak line in WR stars with WC spectrum. It has a very small strength when compared to C II 5891 and a higher excitation potential. On the basis of the arguments given above we consider NaD as the most probable identification of this feature.

Deblending this feature from the wing of He I was not possible for large sections of the orbit because of the very large intensity ratio between the lines. Instead of fitting the profile we used the trailed spectrogram in Fig. 2d and graphically measured the phase shift of NaD relative to He I by overplotting sine

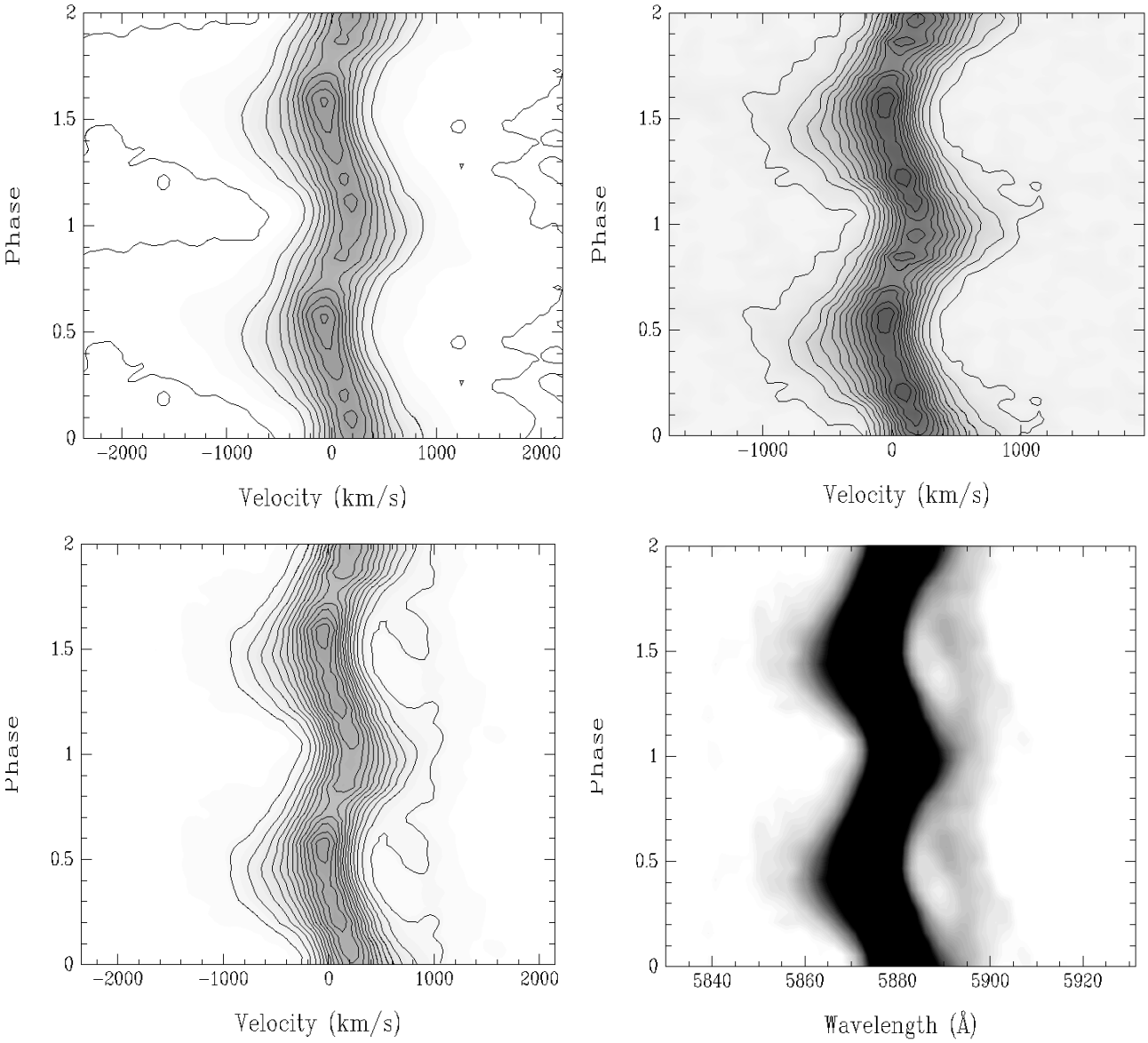

Fig. 2a–d. Trailed spectra of the main emission lines in BL Hyi. The phase scale shown is given by the ephemeris from Eq. 2. Contour lines are linearly spaced from zero to the maximum flux in all panels. **a** Hα is shown with a phase resolution of 0.07 ($FWHM$) and velocity resolution of 160 km s^{-1} ($FWHM$). A logarithmic look-up table was employed in this panel to emphasize the extended line wings. **b** Linear gray scale image of He I 6678 displayed with 220 km s^{-1} ($FWHM$) spectral resolution and 0.07 ($FWHM$) phase resolution. **c** Same as "**b**" for He I 5875. **d** Lower resolution (3.8 Å, 0.09 in orbital phase) image of the He I 5875 region. Note the weak feature near He I 5875 and its phase lag. The linear look-up table was adjusted to enhance this feature.

curves. An estimate of the uncertainty in the procedure was also evaluated as $\sigma_{To} \sim 0.06$ cycles. The following ephemeris is for the time when the NaD radial velocity minus γ changes from negative to positive values:

$$T_0 = 2450379.4725(5) + 0.0789150406\ E \qquad (2)$$

where we used the orbital period quoted in Szkody et al. (1997). The accuracy of the orbital period is superb for folding our data set which comprises only three days from a single observational run. Next we obtained sets of RVs at different positions of the emission line. For that we used a $FWHM_g$ value matching the spectral resolution. Then we constructed diagnostic diagrams for the main emission lines (e.g. Hα shown in Fig. 5). These diagrams show the parameters of the best sinusoid fits to the RV sets as a function of the position of the emission line. The parameter Φ_0 is a measure of the phase shift relative to the ephemeris given by Eq. 2. The main results are:

– Hα: K increases from 140 km s^{-1} in the low velocity regions to 260 km s^{-1} in the high velocity wings. This change is rather smooth and anti-correlated with a decrease of γ by about 30 km s^{-1}. Φ changes by about 0.02 phase units. A mean phase delay of 0.21 cycles is observed.

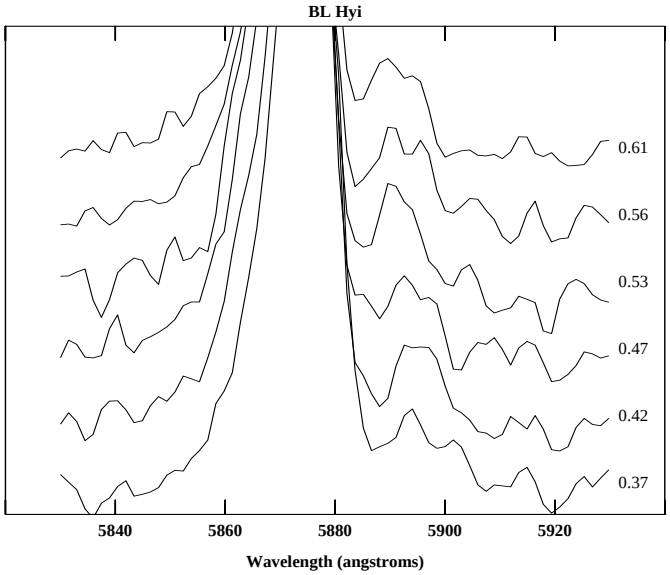

Fig. 3. Phase binned spectra of the He I 5875 region around phase 0.5.

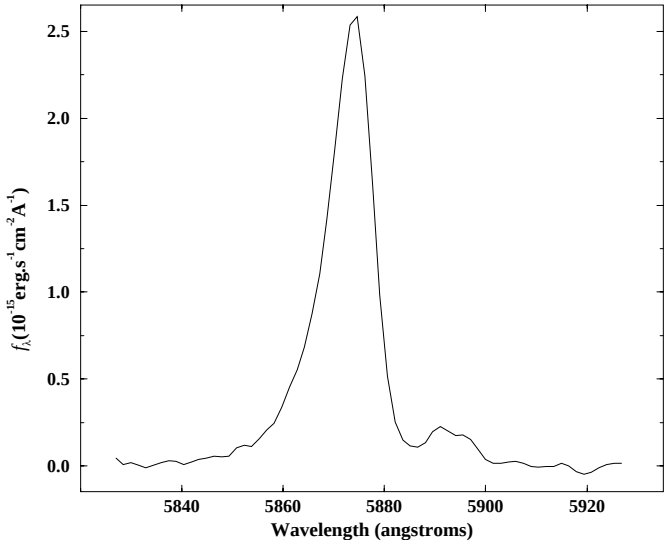

Fig. 4. Average spectrum of the He I 5875 region obtained by shifting the spectra from Fig. 3 by their observed radial velocities (see text).

– He I 5875 and He I 6678: K increases from 130 km s^{-1} in the low velocity regions to 320 km s^{-1} in the high velocity wings. This change is rather smooth and anti-correlated with a decrease of γ by about 26 km s^{-1} (He I 5875) or 42 km s^{-1} (He I 6678). Φ changes by about 0.02 phase units. A mean phase delay of 0.24 cycles is observed.

The above analysis shows no sharp definition between high and low velocity components in our spectra. What is really observed is a smooth transition between high and low velocities when going from the center of the emission to the wings. The phasing of the H I and He I lines is remarkably similar; they precede the Na I D line by about 0.2 cycles.

The RV curves with the lowest σ_K/K values are shown in Fig. 6. The He I 5875 and He I 6678 RV curves are very similar, with small differences with the Hα curve. Previous studies did not test the emission line velocity at different emission line sections. Literature data consist of velocity measurements of the emission line peak, centroid and broad base. For effects of comparison, we will assume that our velocities measured with Δ = 180 km s^{-1} represent the peak velocity and those measured with Δ = 1200 km s^{-1} represent the broad component velocity. Our observations are compared with previous studies in Table 2.

Table 2. Comparison between the results of our line diagnostics and previous studies. K_{peak} and K_{broad}, both in km s^{-1}, are the RV half amplitude of the emission line peak and broad component, respectively (see text). $\Delta\Phi$ is the phase shift between both components. The broad component velocity by H85 was calculated only with Balmer line profiles.

Lines	K_{peak}	K_{broad}	$\Delta\Phi$	Reference
Hα, He I 5875 and He I 6678	133(5)	300(28)	0.02	This work
Hγ, Hδ and He II 4686	142(9)	249(24)	0.02	T83
Hγ, and He II 4686	133(15)	293(20)	0.05	H85

Interestingly, our mean peak velocity (for all lines) closely match the peak velocity found by T83 and H85. Their broad component had mean RV half amplitude similar to our Hα value, but lower than our He I broad component. Also, like in T83 and H85, our broad component leads the peaks for a few hundreds of cycle. However, our results contrast with the observations by T83 and H85 who found the broad component and centroids with higher K velocities than the peaks. We do not have a straightforward interpretation for these differences. However, they may reflect intrinsic differences in the motion of gas in the line emission region during the high photometric state.

3.3. A consistent scenario for the accretion geometry

In this section we show that it is possible to interpretate the multi-wavelength observations of BL Hyi in a consistent way. Several constraints concerning the dipole colatitude and phasing of the column base relative to the light curve features have been published. In this sense, our R light curve is critical to put all the observables in the framework of the absolute phases provided by Eq. 2.

Since this is the first attempt to establish the orientation of the magnetic dipole relative to the secondary star, here we check for possible inconsistencies of our absolute phasing using previously reported multi-wavelength data. Table 3 shows the phases of several observables as given in the literature or measured in this work. As we discuss now, they provide a tentative scenario for the accretion geometry of BL Hyi.

Polarimetric and X-ray studies of BL Hyi suggested the presence of a complex and extended accretion region at the white dwarf, possibly consisting of two active magnetic poles. The definition of such patterns at the accretion regions are not aimed by the present work. However, the column orientation indicated by polarimetry is in agreement with the scenario for the upper accretion column that will be outlined in the next paragraphs.

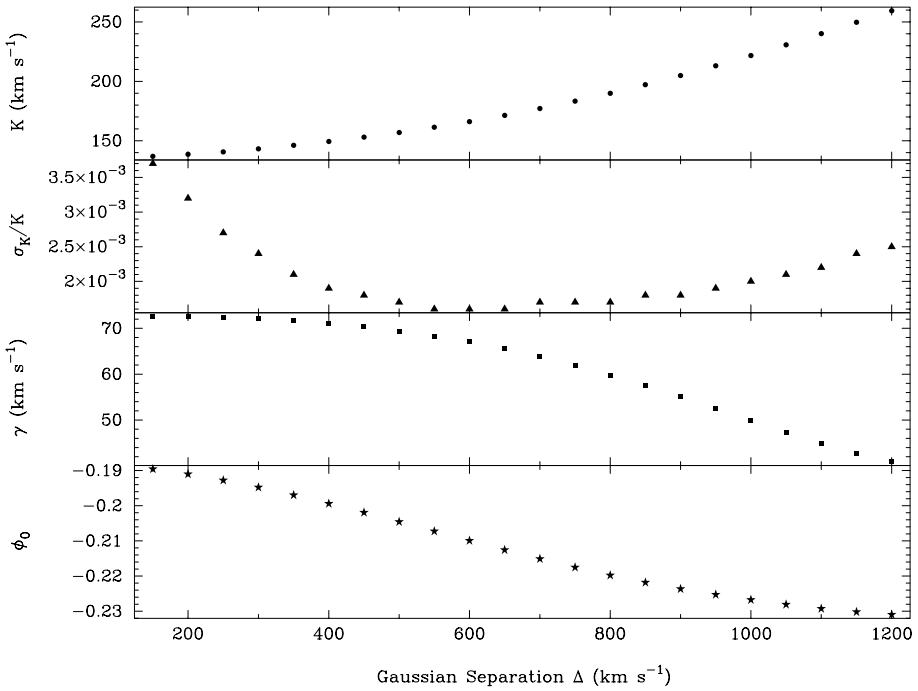

Fig. 5. The diagnostic diagrams for the Hα emission lines. The γ-velocity, the radial velocity semi-amplitude K, the σ_K/K ratio and the phase-shift ϕ_0 are plotted as a function of the Gaussian separation. Phase zero refers to ephemeris given by Eq. 2.

Table 3. Summary of observed quantities constraining the accretion geometry in BL Hyi. The assumed ephemeris is given by Eq. (2).

Observable	Orbital phase	Reference
Radial velocity crossing from negative to positive values	$\equiv 0.0$	This work
Light curve half-rise timing (R band)	0.89	This work
Light curve broad maximum (R band)	1.05–1.15	This work
Minimum radial velocity Hα (wings)	0.55	This work
Minimum radial velocity Hα (core)	0.53	This work
Minimum radial velocity He I 6678 & He I 5876 (wings)	0.50	This work
Light curve broad primary minimum (EUV)	0.25–0.45[a]	Szkody et al. 1997
Light curve dip (EUV)	0.95[a]	Szkody et al. 1997
Light curve broad maximum (0.5–10 keV)	$\sim$ 0.1–0.2[a]	Matt et al. 1998
Light curve half-rise timing (0.5–10 keV)	~ 0.90[a]	Matt et al. 1998
Linear polarization pulse (maximum of main pulse)	~ 1.0[b]	Schwope & Beuermann 1989
Maximum circular polarization (modulus)	~ 0.15[b]	Schwope & Beuermann 1989

[a] These phases rely on an orbital period uncertainty of less than 10^{-6} d for a phase shift smaller than 0.05.
[b] Phase derived from its offset relative to simultaneous optical light curve.

The phase of the linear polarization pulse and maximum circular polarization are consistent with the orbital phase of photometric rise (ϕ=0.89) and maximum ($\phi =\sim$ 1.1). While there is a large uncertainty in the orbital inclination, our spectroscopic observations and phase definition agrees with polarimetry if the dipole longitude (ψ) is between -20 to -70 degrees (i.e. the column projection in the orbital plane lags the secondary by about 0.13 cycles). Observations in the EUV do not fit well in a single accretion spot model. While the dip at phase 0.95 may be tentatively explained by stream absorption, the origin of the main minimum is still unclear (Szkody el al. 1997).

On the other hand, the radial velocity of material falling towards the white dwarf in the stream should has a minimum roughly between phase 0.5 and 0.6, depending on the exact location of emission and the stream angle relative to the line between the stars. Our ephemeris is consistent in the sense that we observe the minimum velocity of all lines at about the expected phase.

3.4. Doppler tomography

Doppler tomography was introduced as a powerful tool in the study of accretion disk kinematics and emission properties by Marsh & Horne (1988). This analysis method is now a widespread procedure in the study of emission lines in CVs, providing a quantitative mapping of optically thin line forming regions in the velocity space. When severe self-absorption and/or intrinsic line broadening are present then the tomograms provide at least a concise and convenient way of displaying phase-resolved line profile measurements. The Doppler recon-

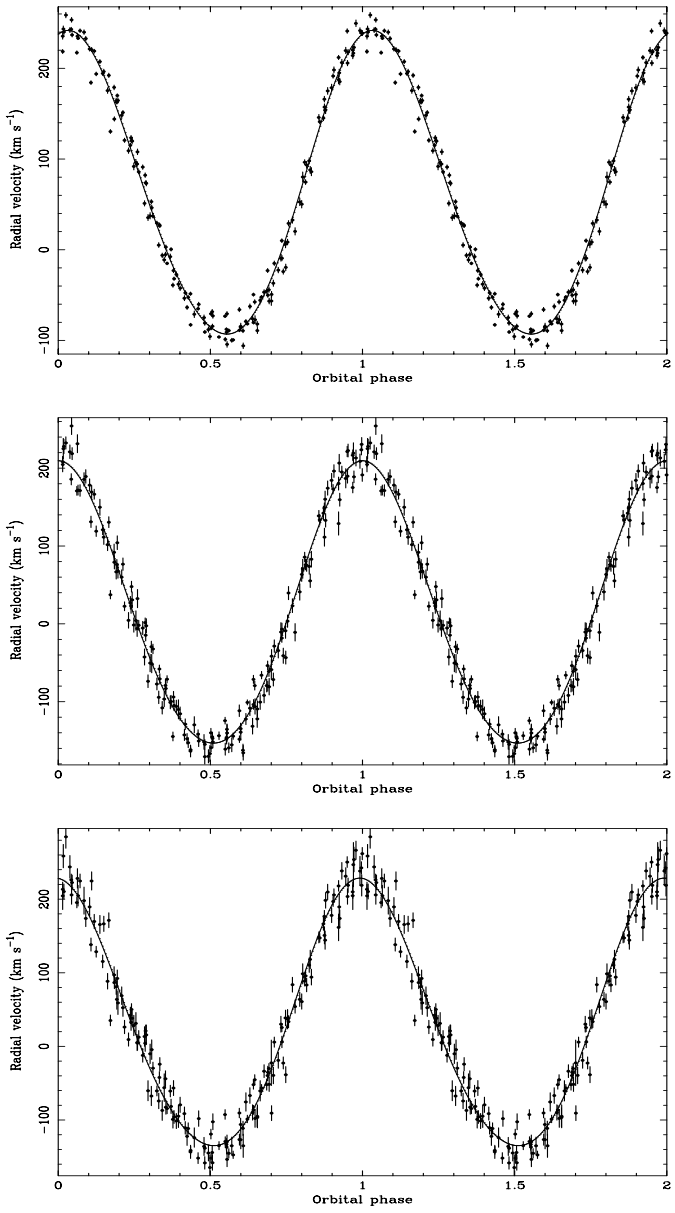

Fig. 6. The Hα (up), He I 5875 (middle) and He I 6678 (below) radial velocities obtained with $\Delta = 600\,\mathrm{km\,s^{-1}}$ and $FWHM_g = 170\,\mathrm{km\,s^{-1}}$. The best sinusoid fits are also shown, and data are shown twice for clarity. Phase zero refers to ephemeris given by Eq. 2.

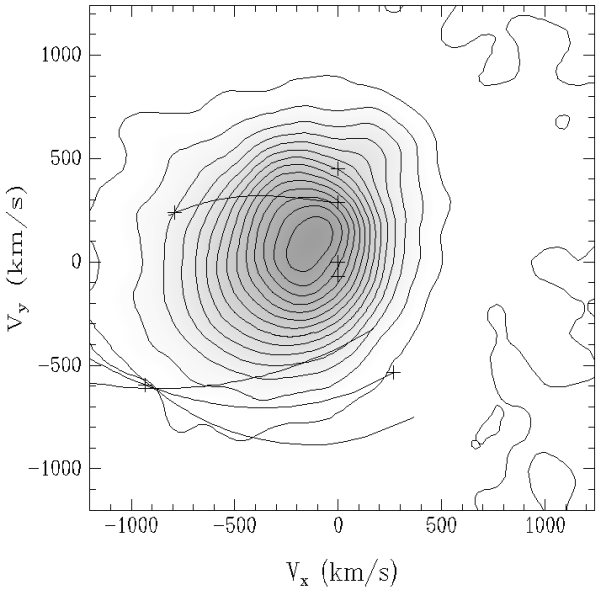

Fig. 7. Doppler map of the Hα emission line. Contour lines are linearly spaced from 0.0 to the maximum emissivity. The expected effective resolution is 170 km s^{-1} (FWHM). The origin ($V_x = V_y = 0$) corresponds to the binary center of mass while the following dynamical informations depend on arbitrary binary parameters ($M_1 = 1.0 M_\odot$, $M_2 = 0.15 M_\odot$ and $i = 45^\circ$) : The plusses along the $V_x = 0$ axis correspond, from top to bottom, to the secondary star, the inner Lagrangian point (L_1), the binary center of mass and the primary star. The curve from L_1 shows the stream path up to the magnetic coupling radius for $\dot{\mathrm{M}} = 4 \times 10^{-11} M_\odot/yr$, $B = 23$ MG and a fractional column area at magnetic coupling radius $f_s = 0.003$. The three curves at the bottom left corner show the expected location of the upper column emission in the velocity space for a dipole geometry with $\beta = 120^\circ$ and $\psi = -60^\circ$. The plusses at the middle curve correspond, from left to right to a column height of 20 $R_w d$ and 30 $R_w d$. A gamma-smearing estimate is given by the separation between the outermost curves in this set (see text).

structions presented in this paper were computed using the filtered backprojection method (Rosenfeld & Kak 1982). The two-dimensional reconstruction of structures in the orbital plane has a unique solution that depends only on the two-dimensional data set (i.e. f_ν (phase, lambda) where f_ν is the flux). The side effect of attempting the mapping of a 3D velocity field is a loss of resolution of structures which have a significant V_z component (Diaz 1993). This happens in polars where the magnetic field axis lies far from the orbital plane. Therefore the emission from gas lifted from the orbital plane in the coupling region as well as the lower part of the accretion column are subject to this method limitation. This effect is often called "gamma-smearing".

In order to interpret the Doppler maps we shall assume that the Na I D line effectively traces the motion of the secondary star. A fiducial absolute phase information is needed in order to have the map axes correctly oriented with respect to the binary system. Our definition follows the usual form; the X-axis points from the primary to the secondary while the Y-axis points in the direction of motion of the secondary. In this case the ephemeris given in Eq. 2 represents the pass of the secondary star along the observer line of sight. If the inferior conjunction estimated from the Na I D feature is in error then the reconstructions would be simply rotated around their centers ($V_x = V_y = 0$) by an angle equal to the absolute error in the conjunction phase. The relative distribution of flux, however, remains unaffected. The maps shown in this sections may be rotated by the corresponding phase shift in face of a further improved absolute ephemeris.

A 23 MG dipole field was combined with a tentative potential well of a 1.0 $M_\odot$ white dwarf and a Roche lobe filling secondary of 0.15 $M_\odot$ to compute the free-fall and magnetically coupled paths in velocity coordinates using the method proposed by Ferrario et al. (1989). Values of the dipole longitude of -60

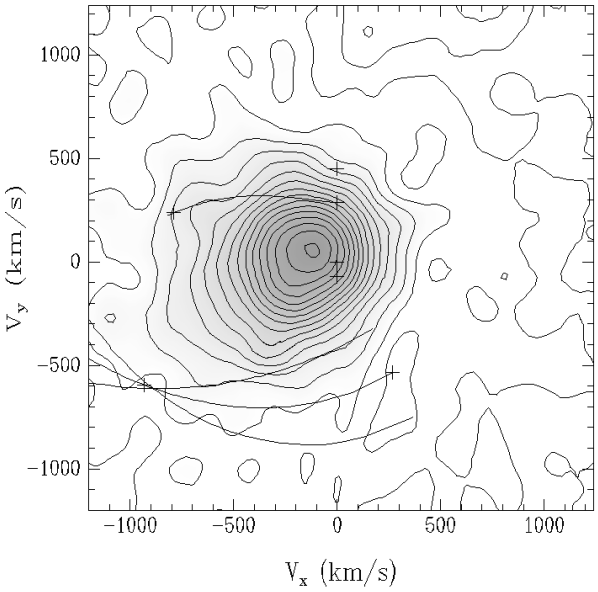

Fig. 8. Same as Fig. 5 for the H I 6678 emission line.

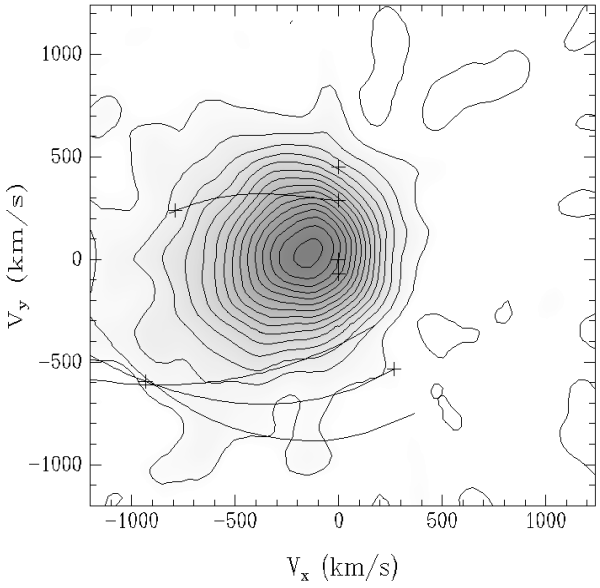

Fig. 9. Same as Fig. 5 for the H I 5875 emission line.

degrees and colatitude of 120 degrees (see Sect. 3.3) were used to derive theoretical "S-wave" components along the column and find its location in the Doppler maps. The gamma velocity of each "S-wave" was then compared to the binary systemic velocity aiming to quantify the possible amount of degradation or gamma smearing in the reconstructions. This effect changes the roughly Gaussian instrumental PSF of the reconstructions into a broader axially symmetric profile with a central depression. The distance between the outermost lines that follow the column path in Fig. 7 indicates the diameter of the degraded PSF. The result indicates an average degradation of less than 600 km s^{-1} for the theoretical column path included in the map velocity range. Although larger than the same effect in VV Pup, it seems unlikely that the gamma smearing alone could prevent the detection of emission from the accretion column in the lower left quadrant of the He I and Hα Doppler images. If a significantly lower white dwarf mass is used in this simulation the column path moves upwards as the magnetic radius increases. In addition, the gamma smearing is also reduced considering the velocity range covered by the reconstructions.

The tomograms of the Hα line shows an extended low-velocity emission located near the ballistic accretion stream (Fig. 7). This feature is responsible for at least 75% of the total line flux. In contrast with the mappings of VV Pup and HU Aqr, the observed emission does not follow the theoretical stream i.e. forming an elongated flux distribution. Instead, the distribution seems "washed" and featureless. The resolution of the maps (180 km s^{-1} FWHM) cannot be blamed for the smoothness of the Doppler images. On the other hand, the data was obtained in a single run and therefore they correspond to a "snapshot" view of the accretion kinematics. We could not detect any narrow emission from the secondary in Hα nor He I.

A comparison between the maps from singlet and triplet helium lines shows that they are extremely similar (Figs. 8 and 9). Line optical depth effects could appear in triplet to singlet rational maps for triplet transitions ending in the 2(3)S level. The main emission structure in these maps is also similar to that observed in the Hα map, it is however slightly shifted towards the secondary in comparison with the Hα map.

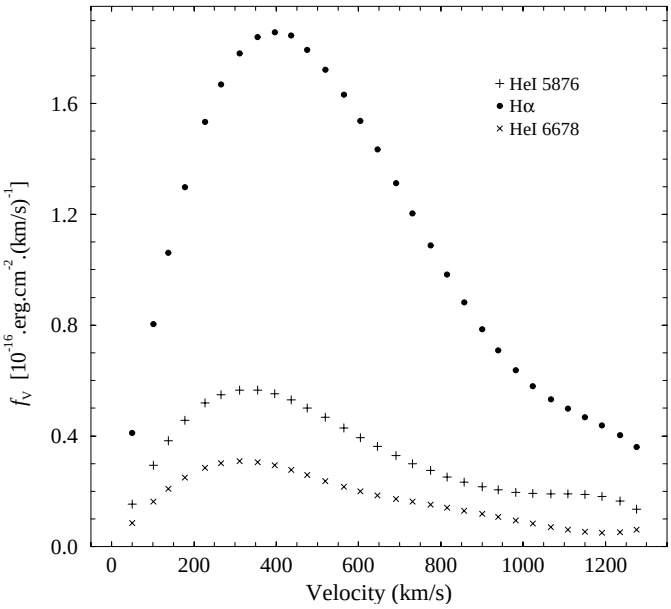

Fig. 10. Line emissivity distributions obtained from full resolution Doppler reconstructions for an inclination of 40 degree (see text).

Our tomograms based on the Na I D lines are too noisy and contaminated by the He I 5875 blend. Tentative reconstructions basically produce a large amorphous feature in the $V_y > 0$ region. The interpretation of the Na I D maps will be avoided due to the low S/N ratio of the profiles and the strong contribution of the He I red wing during a significant part of the orbital cycle.

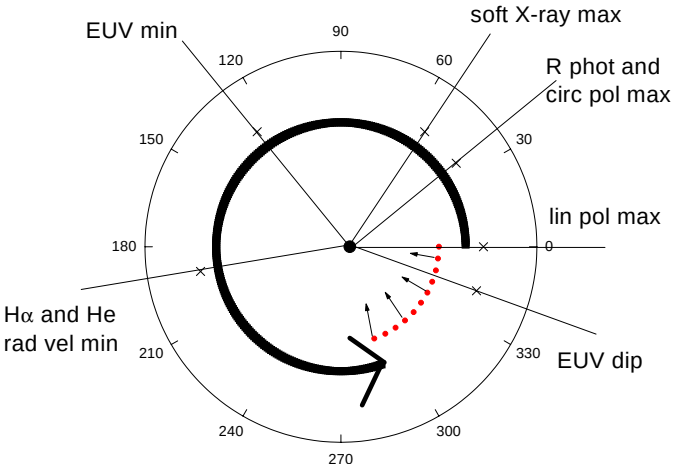

Fig. 11. A diagram showing the phases of detection of the events given in Table 3. The long circular arrow indicates the probable azimuthal extension of the reservoir of low angular momentum gas and their path (projected to the orbital plane), before to be channeled onto the white dwarf. The projected azimuthal extension of the magnetic column is represented by the dots and the small arrows.

3.5. Line emissivity distributions

We calculated the line emissivity as a function of the velocity for the bright emission lines. This quantity is computed directly from the Doppler reconstructions by summing all the flux emitted at a given velocity modulus (or radius) in the tomogram. It has the same units of a line profile but it is free of projection effects. As mentioned before these distributions do not depend on the adopted ephemeris since they depend on the radial coordinate only. The distributions, shown in Fig. 10 steeply rise from low velocities to a maximum and then slowly decrease towards high velocities, in a similar way that the Hα distribution in VV Pup (Diaz & Steiner 1994). Some parameters of these distributions are given in Table 4. They show significant differences only between H I and He I indicating different formation regions for these lines. In both cases, however, the low emissivity at high velocities is conspicuous while its value peaks between 300 km s^{-1} and 400 km s^{-1}. These figures and the two-dimensional distribution seen in the tomograms indicate that the column has a very low emissivity and most He I and Balmer lines are produced at the stream or near the coupling region. This conclusion is independent of the assumed inclination. Even an inclination as low as 30^o changes the velocities by about 28%. However, it seems unlikely that the stream dominates the line production because of the uncharacteristic shape of the Doppler images. If the proposed ephemeris is correct then the accretion column is far away from the orbital plane while the nearest pole azimuth points to a region distant from the $L1$ point and the ballistic stream. Therefore the gas does not feed the accretion funnel directly. Intead, it is lifted from the orbital plane at several white dwarf radius forming an azimutally extended coupling region. This view is sketched in Fig. 11. After migrating in both azimuth and elevation the gas falls to the accretion funnel itself. In this situation the gas may fill a substantial fraction of the Roche volume while get rid of part of its original orbital angular momentum. Such scenario of an extended coupling "buffer" is consistent with the low strength magnetic field and may explain the spread and low-velocity emission seen in the tomograms. Such reservoir of gas should steadily feed the dominant pole through the magnetic field lines during the high photometric states.

Table 4. Parameters of the peaks of the emissivity distributions for an inclination of 40 degrees.

Line	flux (erg cm^{-2} s^{-1})	velocity (km s^{-1})
Hα	1.86E-16	397
He I 5875	5.66E-17	330
He I 6678	3.10E-17	321

4. Conclusions

- Doppler images and line emissivity distributions provided important insights on the nature of the line emission region of BL Hyi.
- Neither the accretion column nor the secondary star seems to contribute – in a significant way – to the H I and He I line emission.
- A subtle emission line near He I 5875 was detected. This line is tentatively identified as Na I D, probably formed in a chromospherically active companion.
- The radial velocity curve of the proposed NaD lines show a significant phase lag when compared to the R.V. curves of all the other emission lines measured in the optical (H I, He I, from this work and He II from Thorstensen et al. 1983).
- Absolute phases for many observables were provided by assuming a secondary's chromospheric activity origin for this line.
- A consistent picture of the accretion geometry of BL Hyi was obtained. This picture fits well within previous optical, polarimetric and X-ray constraints.
- However, the nature of the reported EUV minimum remains unclear.
- A reservoir of low angular momentum gas filling a substantial fraction of the Roche lobe and an accretion column far away from the orbital plane with a magnetic longitude -70 $\leq \psi \leq$ -20 are consistent with our observations.

Acknowledgements. Thanks to an anonymous referee for contributing to improve a first version of this paper. This work was partly supported by Fondecyt 1971064 and DI UdeC 97.11.20-1. Support for this work was also provided by the National Science Foundation through grant number GF-1002-98 from the Association of Universities for Research in Astronomy, Inc., under NSF Cooperative Agreement No. AST-8947990. M.D. acknowledges the support provided by CNPq grant No. 301029 and FAPEMIG grant No. 183696. J.A. acknowledges support by a Gemini-PPARC-FANDES studentship and O.R.S. award.

References

Agrawal P.C., Riegler G.R., Rao A.R., 1983, Nat 301, 318

Beuermann K., Schwope A.D., 1989, A&A 223, 179
Diaz M.P., 1993, Ph.D. Thesis, IAG, Universidade de Sao Paulo
Diaz M.P., Steiner J.E., 1994, A&A 283, 508 (Paper I)
Ferrario L., Tuohy I.R., Wickramasinghe D.T., 1989, ApJ 341, 327
Ferrario L., Bailey J., Wickramasinghe D., 1996, MNRAS 282, 218
Fleming T.A., Schmitt J.H.M.M., Giampapa M.S., 1995, ApJ 450, 401
Horne K., Wade R.A., Szkody P., 1986, MNRAS 219, 791
Hutchings J.B., Cowley A.P., Crampton D., et al., 1982, ApJ 252, 690
Hutchings J.B., Cowley A.P., Crampton D., 1985, PASP 97, 423
Marsh T.R., Horne K., 1988, MNRAS 235, 269
Matt G., Barcaroli R., Belloni T., et al., 1998, A&A 334, 857
Pickles A.J., Visvanathan N., 1983, MNRAS 204, 463
Piirola V., Reiz A., Coyne G.V.S.J., 1987, A&A 185, 189
Ramsay G., Cropper M., Mason K.O., 1996, MNRAS 278, 285
Rosenfeld A., Kak A.C., 1982, Digital Picture Processing. Academic Press, New York, p. 353
Schneider D.P., Young P., 1980, ApJ 238, 946
Schwope A.D., Beuermann K., 1989, A&A 222, 132
Schwope A.D., Beuermann Jordan S., 1995, A&A 301, 447
Schwope A.D., Mantel K., Horne K., 1997, A&A 319, 894
Shafter A.W., 1983, Ph.D. Dissertation, UCLA
Shafter A.W., Reinsch K., Beuermann K., et al., 1995, ApJ 443, 319
Short C.I., Doyle J.G., 1998, A&A 336, 613
Szkody P., Vennes S., Sion E.M., et al., 1997, ApJ 487, 916
Thorstensen J.R., Schommer R.A., Charles P.A., 1983, PASP 95, 140
Tovmassian G.H., Szkody P., Greiner J., et al., 1999, In: Hellier C., Mukai K. (eds.) Annapolis Workshop on Magnetic Cataclysmic Variables. ASP Conference Series Vol. 157, 1999, p. 133
Warner B., 1995, Cataclysmic Variable Stars. Cambridge University Press, Cambridge
Wickramasinghe D.T., Visvanathan N., Tuohy I.R., 1984, ApJ 286, 328
Young P., Schneider D.P., 1979, ApJ 230, 502